ICARUS **130,** 296–312 (1997)
ARTICLE NO. IS975834

Radar Detection of Near-Earth Asteroids 2062 Aten, 2101 Adonis, 3103 Eger, 4544 Xanthus, and 1992 QN

Lance A. M. Benner, Steven J. Ostro, Jon D. Giorgini, Raymond F. Jurgens, David L. Mitchell, Randy Rose, Keith D. Rosema, Martin A. Slade, Ron Winkler, and Donald K. Yeomans

Jet Propulsion Laboratory, California Institute of Technology, Pasadena, California 91109-8099
E-mail: lance@think.jpl.nasa.gov

Donald B. Campbell

National Astronomy and Ionosphere Center, Space Sciences Bldg., Cornell University, Ithaca, New York 14853

and

John F. Chandler and Irwin I. Shapiro

Harvard-Smithsonian Center for Astrophysics, 60 Garden St., Cambridge, Massachusetts 02138

Received March 28, 1997; revised August 28, 1997

We describe Doppler-only radar observations of near-Earth asteroids 2062 Aten, 2101 Adonis, 3103 Eger, 4544 Xanthus, and 1992 QN that were obtained at Arecibo and Goldstone between 1984 and 1996. Estimates of the echo spectral bandwidths, radar cross sections, and circular polarization ratios of these objects constrain their pole-on breadths, radar albedos, surface roughnesses, taxonomic classes, rotation periods, and pole directions. Aten's bandwidth is consistent with its radiometrically determined diameter of 0.9 km. Adonis has a rotation period $P \leq 11$ h and an effective diameter (the diameter of a sphere with the same projected area as the asteroid) between 0.3 and 0.8 km. The radar properties of Adonis suggest it is not a member of taxonomic classes C or M. The effective diameter of Xanthus is between 0.4 and 2.2 km with a rotation period $P \leq 20$ h. Echoes from 1992 QN constrain the asteroid's pole-on breadth to be ≥ 0.6 km and probably exclude it from the C and M taxonomic classes. The strongest Eger echoes are asymmetric with bandwidths that set lower bounds of 1.5 and 2.3 km on the minimum and maximum breadths of the asteroid's pole-on silhouette. If Eger is modeled as a 1.5 × 2.3 km biaxial ellipsoid, then its effective diameter for an equatorial view is 1.5 km end-on and 1.9 km broadside or pole-on, implying a geometric albedo smaller than published values but still consistent with a classification as an E-type object. The near-unity circular polarization ratios of Adonis, Eger, and 1992 QN are among the highest values measured for any asteroid or comet and suggest extreme near-surface roughness at centimeter to meter scales.

Key Words: asteroids; radar; Aten; Adonis; Eger; Xanthus.

1. INTRODUCTION

We report the first radar detections of near-Earth asteroids (NEAs) 2062 Aten, 2101 Adonis, 3103 Eger, 4544 Xanthus, and 1992 QN from observations conducted at Arecibo and Goldstone between 1984 and 1996. Rotation rates, lightcurve amplitudes, visual geometric albedos, and taxonomic classes have been reported for Aten and Eger, but very little is known about the physical properties of Adonis, Xanthus, and 1992 QN (see Table I and references therein). Our observations achieved rather modest signal-to-noise ratios (SNRs) and resolved echoes in Doppler frequency but not, except for Eger, in time delay. Nonetheless, our results offer novel constraints on each target's characteristics. The next section outlines our experimental techniques and then we describe observations in the order Aten, Xanthus, Adonis, 1992 QN, and Eger, corresponding roughly to increasing caliber of the experiments. We then discuss the unusual polarization signatures of Adonis, Eger, and 1992 QN and conclude with prospects for future observations with the upgraded Arecibo radar.

2. OBSERVATIONS

Our observational, reduction, and analysis techniques emulate those described most recently by Mitchell *et al.* (1995) and Ostro *et al.* (1992, 1996b). Table II summarizes key observational parameters. Each observing cycle (run)

0019-1035/97 $25.00

TABLE I
Physical Properties

Asteroid	a (AU)	e	i (°)	H	p_v	D (km)	Class	P (h)	Δm
2062 Aten	0.97	0.183	18.9	17.1[f]	0.2[b,e]	0.9[b,e]	S[a]	40.77[f]	0.26[f]
2101 Adonis	1.87	0.765	1.35	18.7[h]					
3103 Eger	1.41	0.355	20.9	15.2[k,l]	0.53–0.63[j]	1.4–1.5[j]	E[c,j]	5.709[l]	0.7–0.9[c,g,k,l]
4544 Xanthus	1.04	0.250	14.1	17.1[i]					
1992 QN	1.19	0.359	9.59	17.0[d,g]				5.990[g]	1.1[g]

Note. a, e, and i are the semimajor axis, eccentricity, and inclination of the asteroid's orbit. H is the asteroid's absolute visual magnitude, p_v is the geometric albedo, D is the diameter in kilometers, class refers to the taxonomic class (Tholen and Barucci 1989), P is the synodic rotation period in hours, and Δm is the lightcurve amplitude. The taxonomic classes and values of H, p_v, D, P, and Δm were taken from the references indicated.

[a] Gradie (1976).
[b] Cruikshank and Jones (1977).
[c] Gaffey *et al*. (1992).
[d] Marsden (1996).
[e] Morrison *et al*. (1976).
[f] Mottola *et al*. (1995).
[g] Pravec (1996, personal communication).
[h] Tedesco (1990a).
[i] Tedesco (1990b).
[j] Veeder *et al*. (1989).
[k] Wisniewski (1987).
[l] Wisniewski (1991).

consisted of transmission of a circularly polarized continuous wave (cw) for the expected round-trip light travel time for the target, followed by simultaneous reception of echoes for a comparable duration in the opposite (OC) and same (SC) senses of circular polarization. For some observations of Adonis and Eger, linearly polarized waveforms were transmitted and echoes were received in the same-linear (SL) and orthogonal-linear (OL) polarizations. A subset of Eger observations used coarse-resolution binary phase-coded waveforms to determine the asteroid's range.

Our reduction of raw data (echo power spectra) included background removal, calibration, and the formation of sums of spectra weighted by signal strength. In our figures, echo power is plotted vs Doppler frequency, with 0 Hz corresponding to hypothetical echoes from the target's center of mass (COM) [COM frequencies were estimated subjectively; absolute Doppler frequencies were reported by Ostro *et al*. (1991a, 1996a) and are available on the Internet at the JPL Solar System Dynamics website at: http://ssd.jpl.nasa.gov/ (Chamberlin *et al*. 1997)]. Echo power is given by $P_R = P_T G_T G_R \lambda^2 \sigma / (4\pi)^3 R^4$, where P_T is the transmitted power, G_T and G_R are the antenna's gain during transmission and reception, λ is the radar wavelength (equal to 12.6 cm at Arecibo and 3.52 cm at Goldstone), and R is the target's distance. Our figures plot P_R in units of standard deviations of the noise. The radar cross section σ, which can be thought of as the target's radar luminosity, equals 4π times the backscattered power per steradian per unit flux incident at the asteroid and is estimated by integrating power spectra. The circular and linear polarization ratios are $\mu_C = \sigma_{SC}/\sigma_{OC}$ and $\mu_L = \sigma_{OL}/\sigma_{SL}$. μ_C is the more widely used measure of near-surface wavelength-scale roughness (Ostro 1993). Uncertainties in σ are dominated by systematic pointing and calibration errors that are typically between 20 and 50%; due to the low SNR of the observations reported here, we adopt conservative one-standard-deviation errors of 50%. For μ_C and μ_L, systematic effects largely cancel and the remaining statistical errors propagate from receiver noise.

Among observations of near-Earth asteroids reported to date, μ_C has values between ~0.1 and ~1.0 with a mean and rms dispersion of 0.3 ± 0.2 (Ostro *et al*. 1991a) that indicate rougher surfaces than are observed among main-belt asteroids (0.11 ± 0.08; Ostro *et al*. 1985). An object's OC radar albedo is given by

$$\hat{\sigma}_{OC} = \sigma_{OC}/A = 4\sigma_{OC}/\pi D_{eff}^2, \quad (1)$$

where A is the target's projected area and D_{eff} is the effective diameter of a sphere with the same projected area as the target. Published asteroid radar albedos vary from 0.04 for the G-class MBA 1 Ceres (Mitchell *et al*. 1996) to a maximum of 0.58 for the M-class NEA 6178 (1986 DA) (Ostro *et al*. 1991b).

Echo power spectra represent one-dimensional images that can be thought of as brightness scans through a slit parallel to the target's apparent spin vector. The echo's instantaneous bandwidth B is related to the radar wavelength λ and the target's physical properties by

$$B = 4\pi D(\phi) \cos\delta/(\lambda P), \quad (2)$$

where D is the breadth of the plane-of-sky projection of the pole-on silhouette at rotation phase ϕ, P is the apparent rotation period, and δ is the angle between the radar line-of-sight and the object's apparent equator. Expressing B in hertz, D in kilometers, and P in hours gives $D/P = B/27.7 \cos \delta$ for Arecibo and $D/P = B/99.7 \cos \delta$ for Goldstone.

If P is known, then measuring B and setting $\cos \delta = 1$ establishes a lower bound on the asteroid's maximum pole-on breadth D_{max}. If P is unknown (e.g., Adonis and Xanthus), the joint constraint (2) defines a space of possible values of D_{max}, P, and δ. In this case, we find it interesting to consider implications of a *conditional* lower bound on D_{max} that rests on the assumption that the rotation period is at least 4 h, which is true for about 80% of the values reported for NEAs (Chapman *et al.* 1994). This conditional constraint, which we will write as $D_{max}(P \geq 4)$, can be combined with an estimate of radar cross section to make conditional statements about radar/optical albedo and taxonomic type.

Our ability to discern the echo's bandwidth depends on the signal-to-noise ratio, the target's shape, and the radar scattering law. For Adonis, Eger, and 1992 QN we take advantage of their near-unity circular polarization ratios by constructing total power (OC + SC) spectra that increase the SNR by a factor of about $\sqrt{2}$ compared to the SNR for either OC or SC alone. Still, for all our targets, the low SNRs preclude precise measurement of B. Moreover, lacking prior information about target shape and scattering law, it is difficult to assess the accuracy of any plausible spectral-edge estimator. Based in part on experience with modeling echoes from other asteroids, we have chosen to use the "innermost 2-sigma crossings," that is, we take B to be the separation of the frequencies (one lower than the estimated center-of-mass frequency and one higher), where the echo power first drops to two standard devia-

TABLE II
Observations

Target		Date	Observatory	RA (°)	DEC (°)	runs	Δt (UTC hours)	$\Delta\phi$ (°)	Distance (AU)	Setup	POS motion (°)	Pol'n
2062	Aten	1995 Jan 16	G	84.9	33.9	65	02.57 - 11.42	0 - 78	0.130	1.95 Hz	1	C
2101	Adonis	1984 Jul 14	A	138.1	1.5	25	17.28 - 18.99		0.083	0.12 Hz		C
		1984 Jul 15	A	135.1	4.7	21	17.73 - 18.94		0.095	0.12 Hz		C
		1984 Jul 16	A	132.7	7.1	36	16.62 - 18.82		0.107	0.12 Hz	13	C
		1984 Jul 17	A	130.8	9.0	34	16.47 - 18.73		0.120	0.12 Hz		C
		1984 Jul 18	A	129.2	10.6	32	16.13 - 18.61		0.133	0.12 Hz		L
3103	Eger	1986 Jul 16	A	341.8	7.6	12	06.87 - 08.38	0 - 92	0.238	0.61 Hz		C
		1986 Jul 17	A	343.2	7.1	13	07.07 - 08.63	86 - 179	0.230	0.61 Hz		C
		1986 Jul 18	A	344.7	6.5	13	06.99 - 08.49	155 - 246	0.222	0.61 Hz	7	C
		1986 Jul 19	A	346.4	5.8	14	07.06 - 08.63	232 - 329	0.215	0.61 Hz		L
		1986 Jul 20	A	348.0	5.1	14	07.28 - 08.82	319 - 54	0.208	0.61 Hz		L
		1991 Aug 2	G	14.6	-13.0	29	10.55 - 12.16	0 - 98	0.129	0.98 Hz		C
		1991 Aug 5	G	25.7	-18.9	25	13.84 - 15.65	67 - 178	0.124	0.98 Hz	33	C
		1991 Aug 10	G	46.1	-27.4	24	13.96 - 15.78	82 - 193	0.130	0.98 Hz		C
		1996 Jul 29	G	359.0	-7.1	15	08.50 - 09.71	0 - 75	0.133	0.98 Hz	7	C
						18	10.94 - 12.35	154 - 241		5 μs x 12.3 Hz		
						11	14.15 - 14.99	357 - 47		7 μs x 5.86 Hz		
		1996 Jul 30	G	2.2	-9.3	33	10.07 - 12.90	178 - 349	0.129	0.98 Hz		C
4544	Xanthus	1990 Nov 19	A	246.0	21.5	27	15.62 - 18.32		0.173	1.02 Hz	0.2	C
	1992 QN	1996 Jan 11	G	228.6	46.5	31	10.01 - 13.15	0 - 183	0.166	1.95 Hz		C
		1996 Jan 12	G	231.4	44.9	30	10.00 - 12.97	3 - 176	0.164	1.95 Hz	8	C
		1996 Jan 13	G	234.0	43.1	27	10.31 - 13.01	24 - 181	0.163	1.95 Hz		C
		1996 Jan 14	G	236.6	41.3	27	10.34 - 12.99	29 - 183	0.161	1.95 Hz		C

Note. The observations were conducted at Arecibo (A; 2380 MHz) and Goldstone (G; 8510 MHz). Right ascension, declination, and distance are given for each target at the middle of each date's observation. The number of transmit-receive cycles (runs) is listed in the sixth column. Δt is the interval spanned by observations on each date. $\Delta\phi$ is the rotation phase covered on each date, where the start of reception at the beginning of the experiment in a given year defines the zero-phase epoch. The relation between Eger's phase origins in 1986, 1991, and 1996 is unknown. Phase coverage of Adonis and Xanthus is unknown because their rotation periods have not been determined. The tenth column lists the raw cw frequency resolutions in Hz for each object and the raw delay-Doppler resolutions used to range Eger on 1996 July 29. Target plane-of-sky (POS) motion between the first and last day of each experiment is indicated. "C" and "L" denote days devoted to circularly and linearly polarized observations, respectively.

tions. How we treat this 2-sigma bandwidth in discussion of results depends on the SNR and the quality of non-radar information.

3. RESULTS

2062 ATEN (*1976 AA*)

Aten was discovered by E. F. Helin at Palomar in 1976 and was the first known asteroid with a semimajor axis of less than 1 AU (Helin and Shoemaker 1977). Aten's diameter and V-filter visual geometric albedo were inferred from infrared radiometry by Morrison *et al.* (1976) to be 900 ± 200 m and 0.2 ± 0.07, respectively, making Aten the smallest known asteroid at the time of its discovery. Cruikshank and Jones (1977) obtained consistent diameter and geometric albedo estimates of 940^{+200}_{-100} m and 0.18 ± 0.06. Photometric colors measured by Gradie (1976) and the albedo estimates associate Aten with the S taxonomic class. Mottola *et al.* (1995) measured Aten's lightcurve and found an amplitude of 0.26 magnitudes, indicative of an object that is not substantially elongated, and an unusually long rotation period of 40.77 ± 0.20 h. Table I summarizes Aten's *a priori* properties.

We observed Aten on a single night (Table II) at a frequency resolution of 1.95 Hz. An OC weighted sum from all 65 cw runs (Fig. 1) shows a 20-sigma echo in one resolution cell and a 4.5-sigma point next to it. The *a priori* values of P and D predict an echo bandwidth of 2.3 cos δ Hz, consistent with our result. We estimate radar cross sections: σ_{OC} = 0.082 km^2 and σ_{SC} = 0.032 km^2 (Table III), yielding a circular polarization ratio, μ_C = 0.39 ± 0.06, that signifies a surface that is rough at decimeter scales. Aten's polarization ratio is comparable to those of 1862 Apollo (μ_C = 0.4) and 3199 Nefertiti (μ_C = 0.47), and exceeds ~70% of the polarization ratios among all radar-detected NEAs (Ostro *et al.* 1991a, Ostro 1993). If we take D_{eff} to be 0.94 km, then Aten's radar albedo is about 0.12, comparable to the average value estimated for other S-class asteroids (0.16 ± 0.07)(Ostro *et al* 1991b).

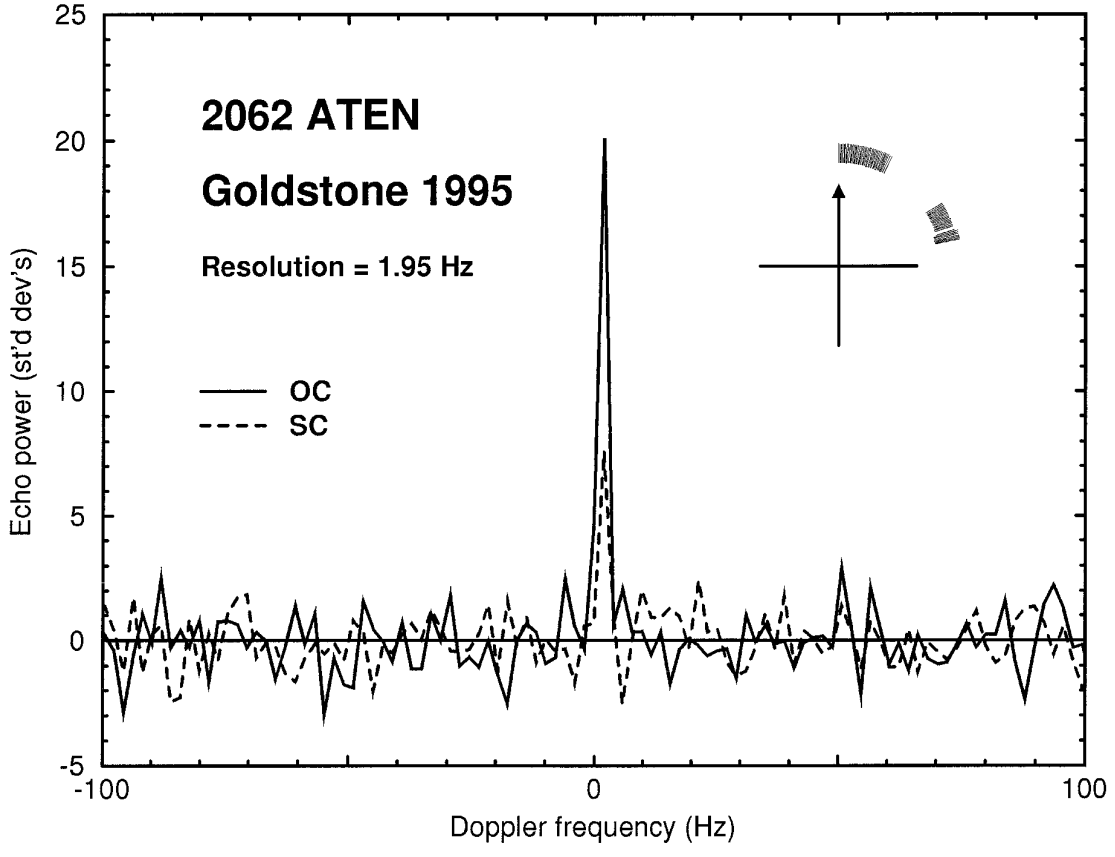

FIG. 1. Goldstone echo power spectrum of Aten at the raw resolution of 1.95 Hz. Echo power is plotted in standard deviations versus Doppler frequency relative to the frequency of echoes from the asteroid's center of mass. Solid and dashed lines denote echo power in the OC and SC polarizations. An inset cross indicates rotational phase coverage based on an apparent rotation period of 40.77 h, where the arrow denotes the zero-phase UTC epoch of 1995 January 16 02:37:09 and phase increases clockwise. Lengths of the radial line segments are proportional to the standard deviation of each spectrum included in the sum.

TABLE III
Radar Properties

Target		OC SNR	B (Hz)	$\sigma_{OC} \pm 50\%$ (km^2)	μ_C	μ_L	$\hat{\sigma}_{OC}$
2062	Aten (G)	20	< 4	0.082	0.39 ± 0.056		≤ 0.18
2101	Adonis (A)	13	2	0.02	1.03 ± 0.11		≤ 0.45
	Jul 14	5	1	0.017	1.11 ± 0.20		
	Jul 15	7	2	0.021	0.91 ± 0.16		
	Jul 16	8	1	0.020	1.03 ± 0.15		
	Jul 17	7	2	0.029	0.88 ± 0.14		
	Jul 18		2			0.0 ± 0.2	
3103	Eger (A: 1986)	13	9	0.62	0.80 ± 0.11	0.26 ± 0.14	≤ 0.33
	Eger (G: 1991)	26	39	0.57	0.94 ± 0.05		≤ 0.30
	Aug 2	10	29	0.35	1.22 ± 0.14		
	Aug 5	22	39	0.81	0.89 ± 0.06		
	Aug 10	15	24	0.62	0.79 ± 0.08		
	Eger (G: 1996)	30	40	0.48	1.02 ± 0.05		≤ 0.26
	Jul 29	15	36	0.50	1.13 ± 0.10		
	Jul 30	26	40	0.47	1.03 ± 0.06		
4544	Xanthus (A)	8	3	0.15	0.07 ± 0.12		≤ 1.5
	1992 QN (G)	8	10	0.086	1.1 ± 0.19		≤ 0.45
	TX RCP (Jan 11 & 12)	5	8	0.073	1.2 ± 0.36		
	TX LCP (Jan 13 & 14)	6	10	0.082	1.1 ± 0.28		

Note. Radar properties of each target, determined from weighted sums of cw spectra. OC SNR is the OC signal-to-noise ratio obtained from an optimally filtered weighted spectral sum. B is the echo bandwidth. The bandwidths of Eger were obtained from spectra spanning ~90° of rotation to avoid smear due to Eger's asymmetric shape. σ_{OC} is the OC radar cross section; assigned uncertainties are the root sum square of systematic calibration errors and are estimated to be ≤50% of the radar cross section. μ_C is the circular polarization ratio σ_{SC}/σ_{OC}, and $\mu_L = \sigma_{OL}/\sigma_{SL}$ is the linear polarization ratio, where uncertainties are statistical fluctuations due to receiver noise. $\hat{\sigma}_{OC}$ is the OC radar albedo computed from 1-sigma upper limits in σ_{OC}. Observations of 1992 QN on January 11–12 and 13–14 used right (RCP) and left (LCP) circularly polarized transmissions, respectively (see text).

4544 XANTHUS (1989 FB)

We observed Xanthus 20 months after it was discovered by H. E. Holt and N. G. Thomas at Palomar (Shoemaker *et al.* 1989). Figure 2 shows weighted sums of our 27 echo power spectra both at the raw resolution of 1 Hz and smoothed to an effective frequency resolution of 4 Hz. Our estimated polarization ratio, $\mu_C = 0.07 \pm 0.12$, is near the low end of the distribution of NEA values. Lacking information about the asteroid's diameter, rotation period, and spin vector, we use Xanthus' 2-sigma-crossing bandwidth of 3 Hz to set a conditional lower bound on its maximum pole-on breadth: $D_{max}(P \geq 4) \geq 0.43$ km. This result and the 1-sigma uncertainty in our estimated radar cross section, $\sigma_{OC} = 0.15$ km^2, place an upper bound on the radar albedo, $\hat{\sigma}_{OC} \leq 1.5$, that is too high to be very interesting.

Figure 3 shows how the radar albedo and visual geometric albedo p_v of Xanthus depend on its effective diameter. The figure also indicates representative values of p_v for principal taxonomic classes and condenses information about the distribution of estimates of other asteroid radar albedos. Optical geometric albedos as a function of diameter and absolute magnitude H were computed using (Zellner 1979)

$$\log p_v = 6.244 - 2 \log D - 0.4H. \quad (3)$$

Radar albedos between 0.04 and 0.3 bound ~90% of known asteroid radar albedos (Ostro *et al.* 1991b) and indicate the most likely range for the radar albedo of Xanthus. A radar albedo of 0.04, the lowest yet reported for an asteroid (Ceres, Mitchell *et al.* 1996), would correspond to $D_{eff} = 2.2$ km and a C-class geometric albedo of 0.05. Substituting that diameter into Eq. (2) produces a rotation period $P \leq 20$ h, a limit that encompasses ~80% of known NEA rotation rates. Unless Xanthus has an exceptionally low radar albedo <0.04, its diameter is most likely between 0.4 and 2.2 km. The corresponding range of geometric albedos

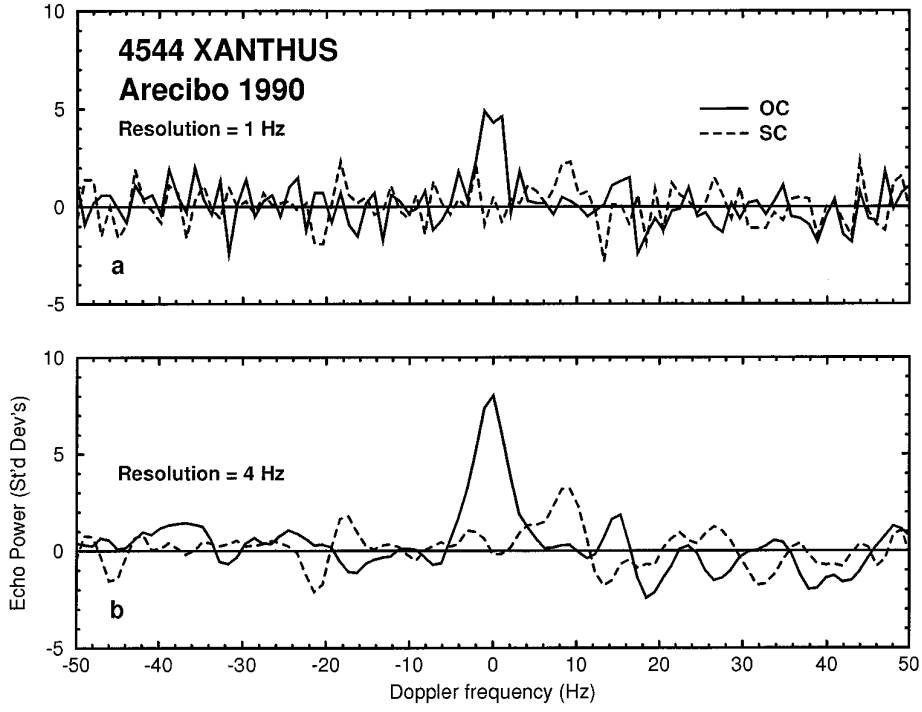

FIG. 2. Xanthus echo spectra.

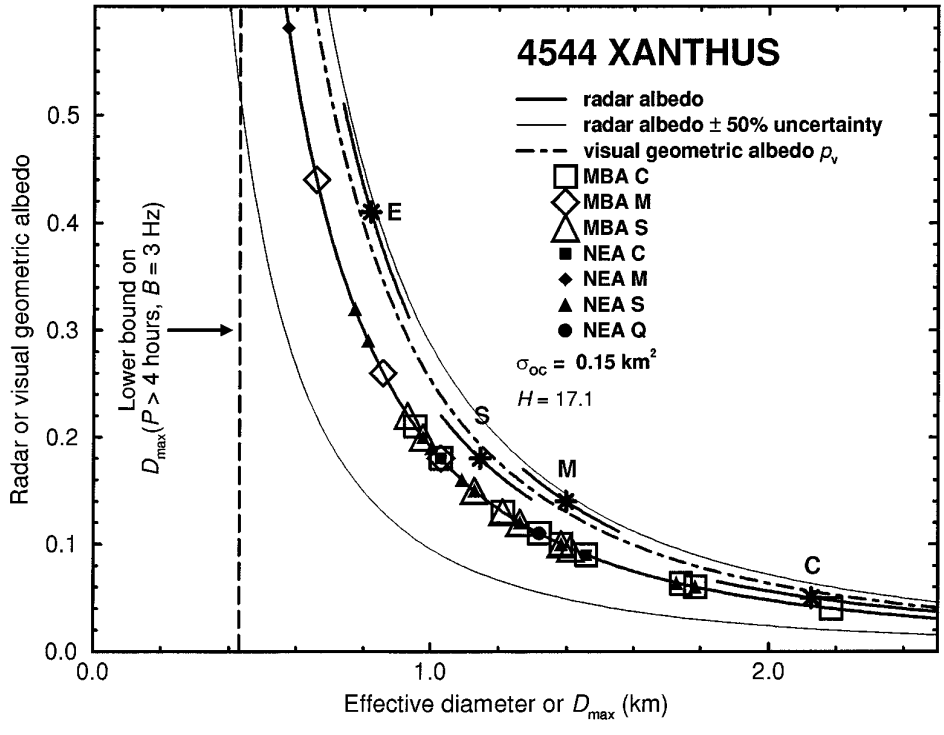

FIG. 3. Constraints on the diameter, radar albedo, and visual geometric albedo of Xanthus. Radar albedo appears as a thick solid curve that is computed from Eq. 1 and Xanthus' radar cross section (Table III). Thin solid curves denote estimated 1-sigma uncertainty in $\hat{\sigma}_{OC}$ that propagates from uncertainty in σ_{OC}. Superimposed on the radar albedo curve and plotted solely as a function of radar albedo is the distribution by taxonomic class of main-belt and near-Earth asteroid radar albedos. Allowed geometric albedos are shown (dash–dot curve) and were computed as a function of diameter using Xanthus' absolute magnitude (Table I) and Eq. 3; mean and rms dispersions of the geometric albedos for the C, M, S, and E taxonomic classes (Tedesco 1989) are indicated by asterisks and adjacent thick curves. A vertical dashed line at $D_{max} = 0.43$ km marks a conditional lower bound on Xanthus' pole-on breadth based on its bandwidth (Table III) and a rotation period assumed to be at least 4 h.

TABLE IV
Radar Constraints on Physical Properties

Target	D_{max} (km) (lower bound)	D_{eff} (km) (upper bound)	P_{max} (h) (upper bound)	p_v (upper bound)
2062 Aten		1.6		
2101 Adonis	0.3	0.8	11	0.7
3103 Eger	2.3	3.9		0.5
4544 Xanthus	0.4	2.2	20	1.4
1992 QN	0.6	1.7		0.8

Note. D_{max} is the asteroid's maximum pole-on breadth determined from its bandwidth and rotation period; for Adonis and Xanthus, conditional rotation periods of at least 4 h were assumed. D_{eff} is the effective diameter determined from the radar cross section and an assumed radar albedo of 0.04. P_{max} is the rotation period of Adonis and Xanthus derived from their radar cross sections and the assumption that their radar albedos are greater than 0.04. p_v is the optical geometric albedo derived from D_{max} (equated with D_{eff}) and the target's absolute magnitude (Table I) except for Eger, where we have adopted an upper limit on p_v estimated from a biaxial ellipsoid model (see text).

encompasses taxonomic classes E, S, M, and C. Table IV summarizes radar constraints on the physical properties of Xanthus.

2101 ADONIS (1936 CA)

Figure 4 shows weighted sums of echo spectra at the raw resolution of 0.12 Hz from the four days of circular polarization observations and the single day of linear-polarization observations. Figure 5 shows single-date sums smoothed to 1-Hz resolution. We cannot see any significant day-to-day variations in echo bandwidth, spectral shape, or circular polarization ratio (Table III).

We use Adonis' 2-sigma-crossing bandwidth of 2 Hz to set a conditional lower bound on its maximum pole-on breadth: $D_{max}(P \geq 4) \geq 0.3$ km. The weighted sum of all OC spectra provides an estimate of Adonis' radar cross section, $\sigma_{OC} = 0.02$ km^2, that is comparable to the smallest asteroid radar cross sections measured (Ostro *et al.* 1991a, Ostro 1993). Treating D_{max} as D_{eff} and adopting the 1-sigma uncertainty in σ_{OC} sets an upper bound of 0.45 on Adonis' radar albedo that encompasses ~95% of reported NEA radar albedos.

Figure 6 shows how Adonis' radar albedo and visual geometric albedo depend on its effective diameter. If the radar albedo of Adonis is at least as large as that of Ceres (0.04), then $D_{eff} < 0.8$ km and (let us continue to equate D_{max} to D_{eff}) Eq. 2 dictates that $P < 11$ h (Table IV). Adonis' radar cross section and absolute magnitude are consistent with taxonomic classes E and S, but suggest that Adonis' radar albedo is less than ~0.1 if Adonis belongs to the M-class and that its radar albedo is less than that of Ceres if Adonis is a C-class object.

Surprisingly high circular polarization ratios near unity were obtained on each of four consecutive days (Fig. 5; Table III). Hoping to constrain theoretical interpretations

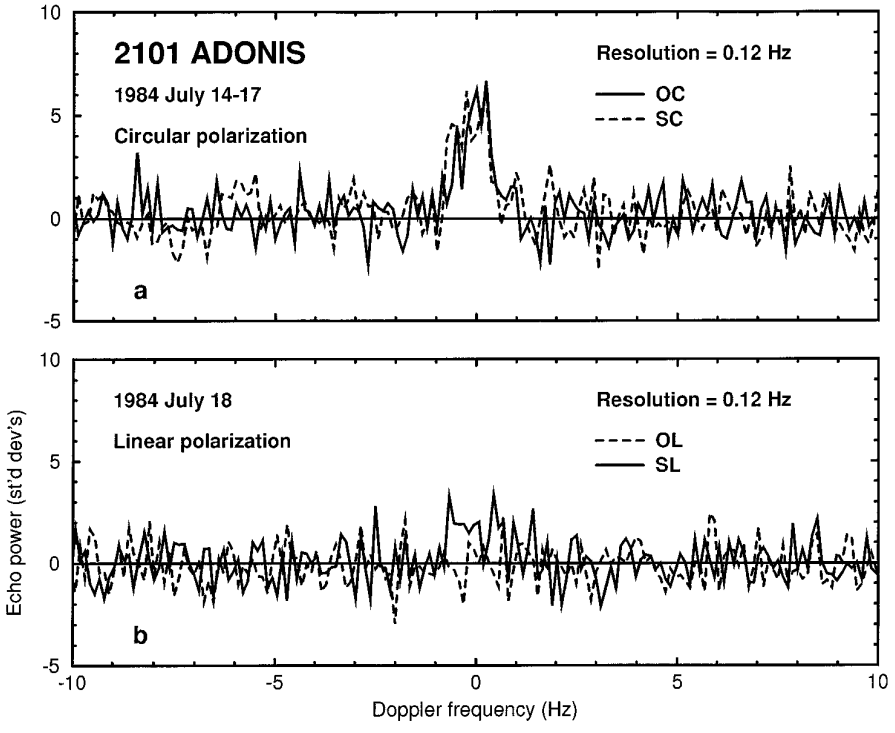

FIG. 4. Adonis echo spectra.

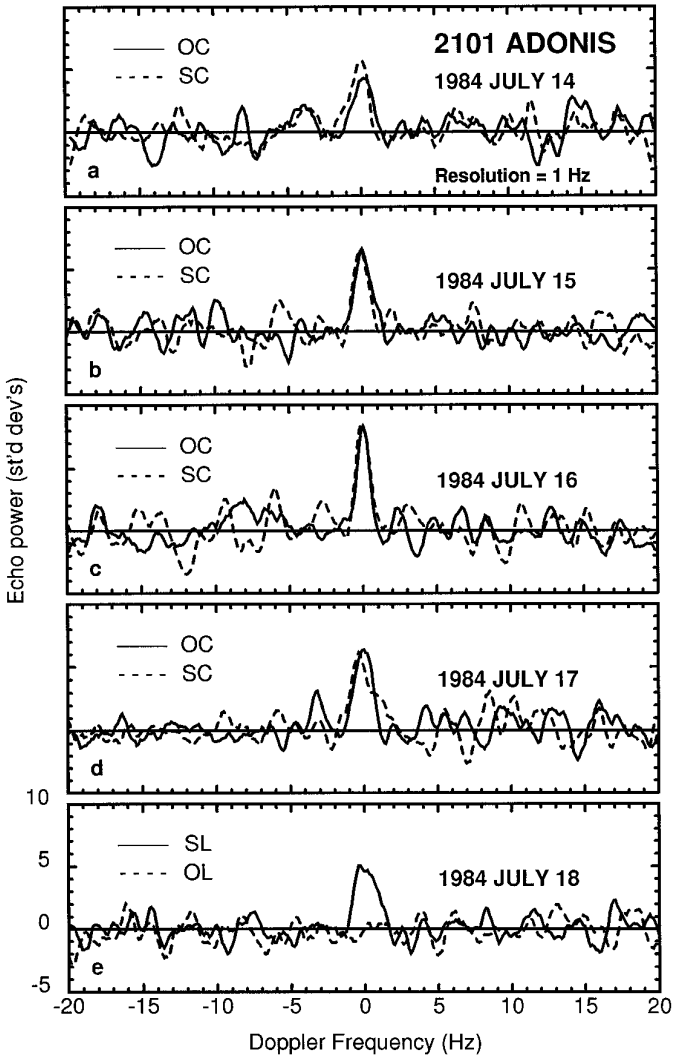

FIG. 5. Single-date sums of Adonis spectra.

of the high values of μ_C, we did dual-linear-polarization observations on the last day of the experiment and obtained the result: $\mu_L = 0.0 \pm 0.2$. We defer discussion of Adonis' polarization signature to Section 4.

1992 QN

A weighted, smoothed sum of the 113 useful OC and SC spectral pairs from four consecutive observation days shows echoes at the 8-sigma level when smoothed to 8-Hz resolution (Fig. 7) and yields a radar cross section of $\sigma_{OC} = 0.086$ km^2 (Table III). We estimate 1992 QN's total-power bandwidth to be at least 10 Hz, which, using 1992 QN's rotation period of 5.990 hours (P. Pravec, personal communication; http://sunkl.asu.cas.cz/~ppravec/neo.html) and Eq. 2 sets a lower bound of $D_{max} \geq 0.6$ km (Table IV).

Figure 8 shows the range of diameters and albedos that are consistent with 1992 QN's radar cross section and absolute magnitude. The 1-sigma uncertainty in our radar cross section and the lower bound on D_{max} set an upper bound on the radar albedo: $\hat{\sigma}_{OC} \leq 0.45$. This constraint encompasses all reported asteroid radar albedos except that of M-class asteroid 6178 (1986 DA) ($\hat{\sigma}_{OC} = 0.58$) (Ostro *et al.* 1991b). If 1992 QN is an M-class object, then its radar cross section indicates that its radar albedo is less than the lowest value measured for that class, $\hat{\sigma}_{OC} = 0.18$ for MBA 97 Klotho (Ostro *et al.* 1991b). If 1992 QN is a C-class object, then its radar albedo is less than that of Ceres. If 1992 QN has a radar albedo >0.04, then its effective diameter is unlikely to exceed about 1.7 km.

The first two days of this experiment used right circular polarization (RCP) transmissions and simultaneous reception of left circular polarization (LCP) and RCP, and yielded a surprisingly high SC/OC ratio of 1.1 + 0.19. On the last two days, we used LCP transmission and simultaneous reception of LCP and RCP and obtained consistent results (Table III), strengthening confidence that there were no "hidden" sources of systematic error in estimation of μ_C. We discuss this asteroid's polarization signature in Section 4.

3103 EGER (1982 BB)

Eger is the only known E-class near-Earth asteroid (Veeder *et al.* 1989) and it may be the parent body of the enstatite achondrite meteorites (aubrites) (Gaffey *et al.* 1992, see also Meisel *et al.* 1995). Photometry by Wisniewski (1987, 1991) and Pravec (1996, personal communication) yielded synodic rotation periods of 5.71, 5.709, and 5.706 h, respectively, and lightcurve amplitudes between 0.7 and 0.9 magnitudes (Table I). Here we adopt the most recently published value for Eger's rotation period (Wisniewski 1991). Gaffey *et al.* (1992) suggested that Eger's lightcurve amplitude is indicative of an elongated body with an aspect ratio of ~2.3. The alternative hypothesis that the lightcurve amplitude arises from large-scale albedo variations is not supported by the Gaffey *et al.* infrared lightcurve.

We observed Eger at Arecibo in July 1986 and at Goldstone in August 1991 and July 1996 (Table II), intervals of almost exactly 5 years due to a 3 : 5 mean motion resonance between the orbits of Eger and Earth (Milani *et al.* 1989). The Table III estimates of μ_C agree within their standard errors and the average OC radar cross sections estimated in the 3 years are consistent within our assigned 50% uncertainty. Hoping to constrain interpretations of the high values of μ_C, we did dual-linear-polarization observations on the last two days of the 1986 experiment (see Section 4).

Figure 9 shows separate weighted sums of the circular and linear polarization data from 1986. The 1991 and 1996 data sets are much stronger, and for these Figs. 10, 11, 12, and 14 show weighted sums of data sorted by date and rotation phase.

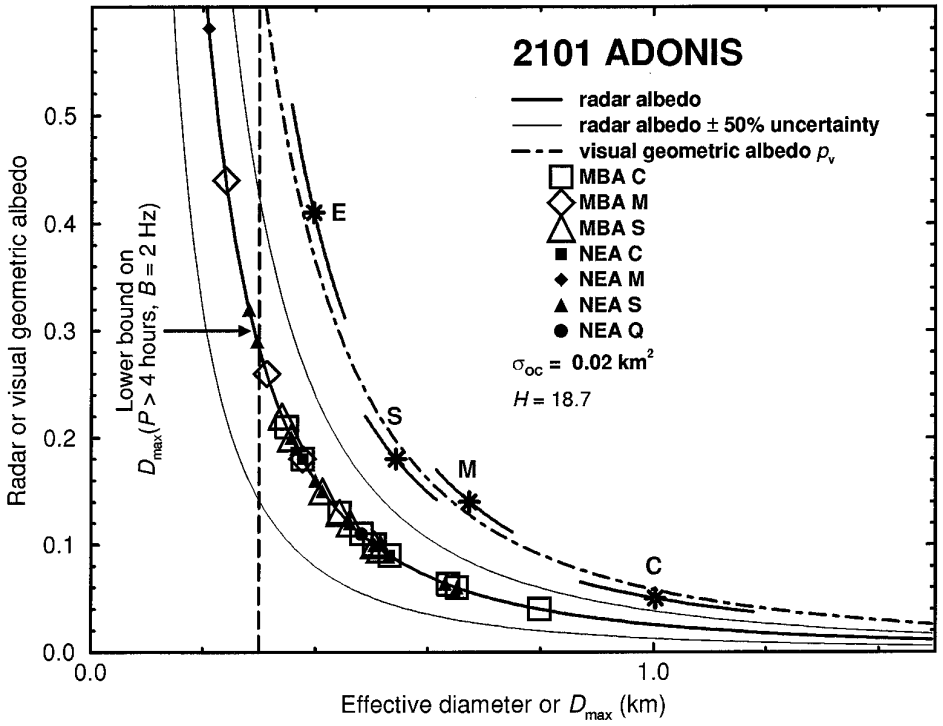

FIG. 6. Constraints on Adonis' diameter and radar and geometric albedos. Adonis' bandwidth (Table III) and an assumed rotation period $P \geq 4$ h establish conditional lower and upper bounds of $D_{max} \geq 0.3$ km and $\hat{\sigma}_{OC} \leq 0.3$.

Figure 13 shows total power spectra obtained on opposite sides of Eger in 1996. These asymmetric spectra are almost mirror images of each other, as would be expected for low-subradar-latitude views of an asymmetric object with a rough-surface scattering law. Eger's 1996 2-sigma bandwidth varies between 40 and 27 Hz as the asteroid rotates (Fig. 14), corresponding to a pole-on elongation of about 1.5 (somewhat less than proposed by Gaffey *et al.* 1992) and pole-on dimensions $\sim(1.5 \times 2.3)$ km/cos δ. Several sums over 30° of phase (Figs. 12c, 14a, and 14f) display a modest deficit of echo power at their centers that may represent a surface concavity.

Figure 15 shows echo power spectra that were extracted from two low-resolution delay-Doppler images obtained on July 29. The spectral bandwidths, shapes, and apparent edge frequencies in Fig. 15 are consistent with those seen in 1-Hz-resolution spectra covering the same rotation phases (Fig. 13), and the apparent delay extent of two 750-m range "gates" is consistent with Eger's cw bandwidth and rotation period.

Let us consider some possible implications of our 2-sigma-crossing constraint on Eger's dimensions. Lacking constraints on Eger's third dimension, we model Eger as a 1.5×2.3 km biaxial ellipsoid, which has an effective

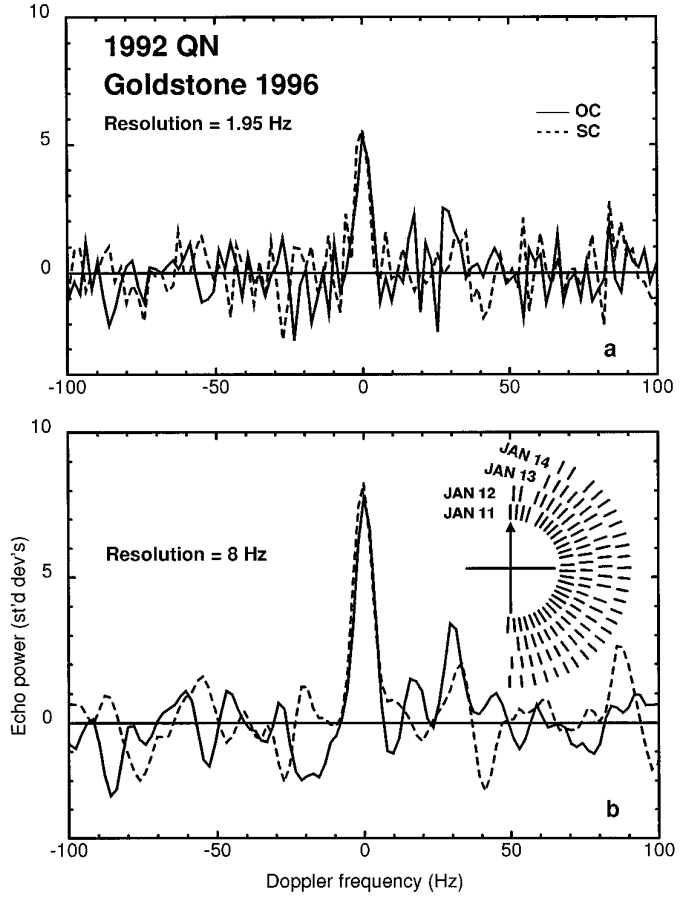

FIG. 7. 1992 QN echo spectra. Phase coverage is indicated for each day, where the initial UTC epoch is 1996 January 11 10:04:16.

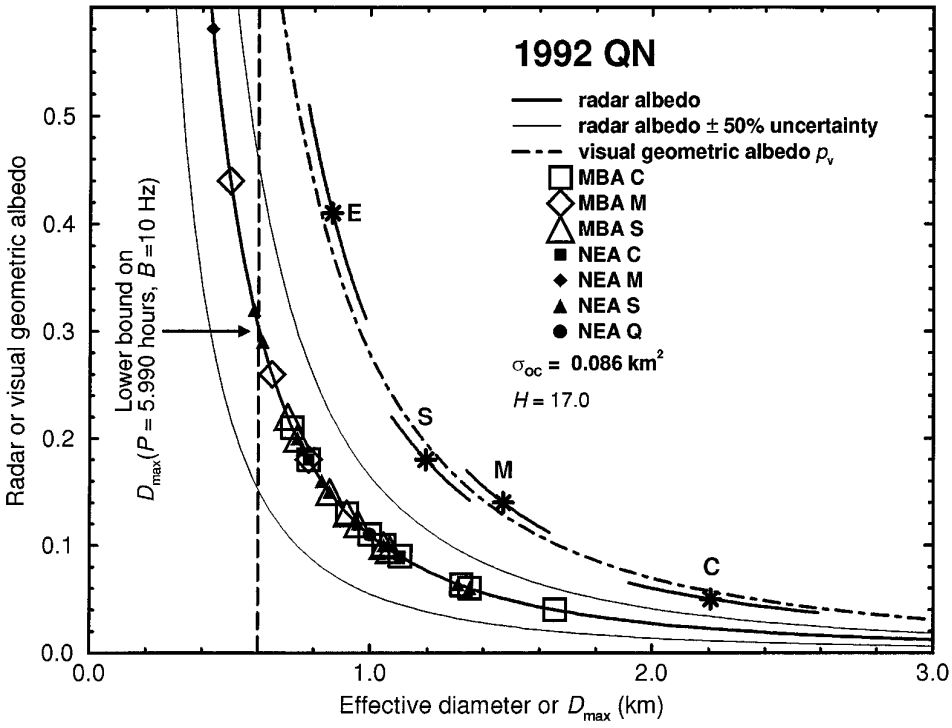

FIG. 8. Constraints on 1992 QN's diameter and radar and visual geometric albedos. The vertical dashed line at D_{max} = 0.6 km is a lower bound on 1992 QN's pole-on breadth determined by its bandwidth and apparent rotation period (Table III).

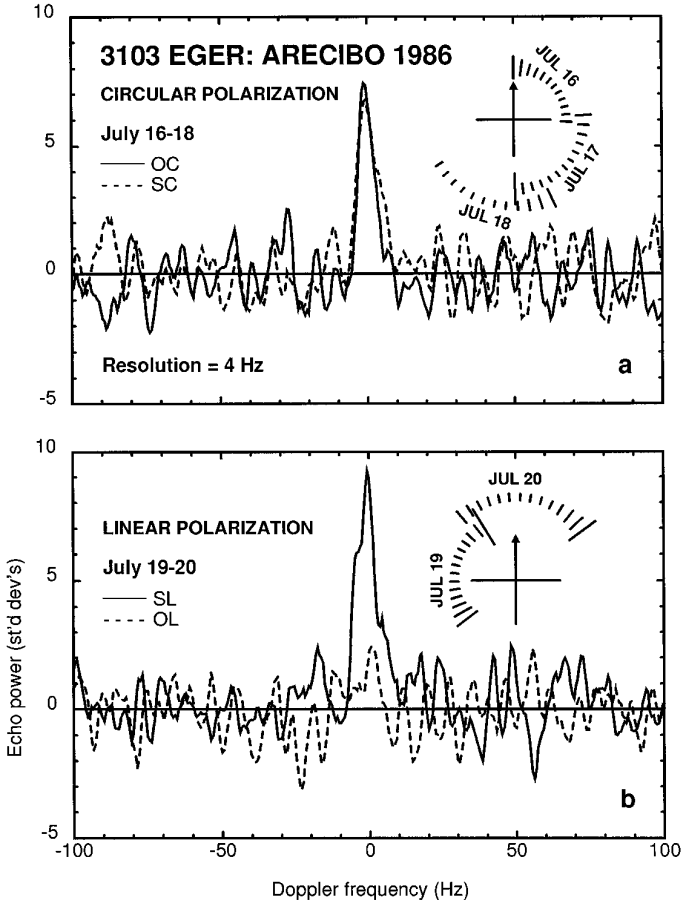

diameter (for an equatorial view) of 1.5 km end-on and 1.9 km broadside or pole-on, both exceeding the Veeder *et al.* (1989) result, 1.4–1.5 km. For this simple model, upper bounds on Eger's visual geometric albedo are 0.53 end-on and 0.34 broadside or pole-on, implying that the radiometrically-determined geometric albedos of 0.53–0.63 obtained by Veeder *et al.* (1989) may be too high. This conditional reduction in geometric albedo is insufficient to change Eger's taxonomy to the M-class (Fig. 16), which is characterized by geometric albedos between 0.08 and 0.20 and a mean and rms dispersion of 0.14 and 0.03, respectively (Tedesco 1989). If Eger *were* an M-class asteroid, then its radar albedo would likely be less than 0.1 and the lowest measured for that taxonomic class (Fig. 16). Thus Eger's E-classification seems secure.

If our echoes were much stronger, Eger's 71° angular motion during our observations (Fig. 17) would provide tight constraints on its spin vector. As noted above, the 1996 signature argues for a low subradar latitude. Also, there are hints that the bandwidth within a given rotation-phase block narrowed from August 5 to August 10, 1991 (Fig. 10b, 10c, 12d, 12e). That progression presumably corresponds to a more pole-on view.

FIG. 9. Eger echo spectra from 1986. Rotational phase coverage is shown for each day relative to an arbitrary zero-phase UTC epoch of 1986 July 16 06:52:10.

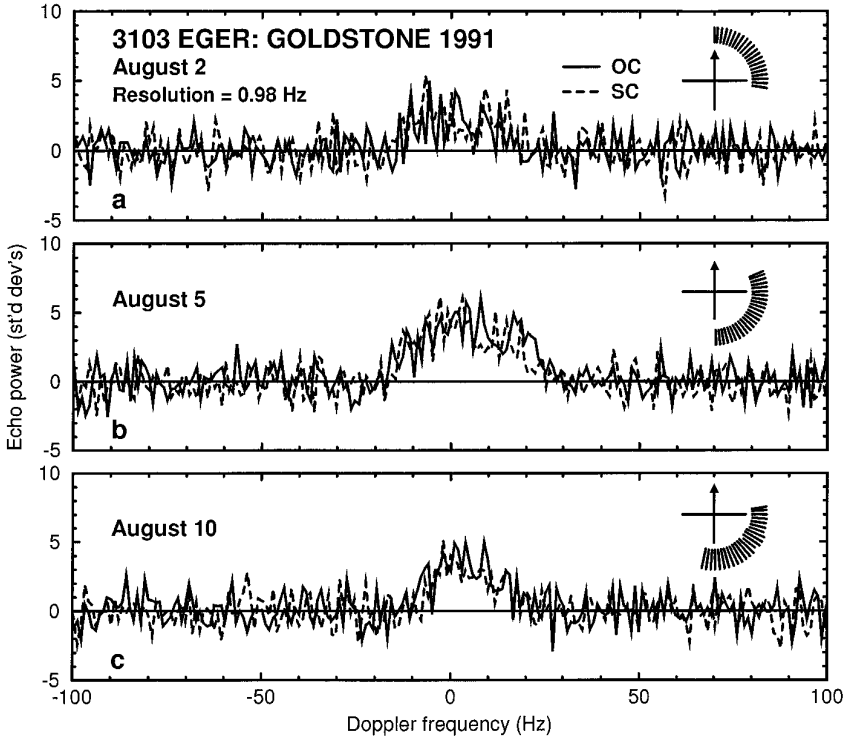

FIG. 10. Eger echo spectra from 1991. The zero-phase UTC epoch is 1991 August 2 10:33:09. The relation between our zero-phase epochs in 1986 and 1991 is not known.

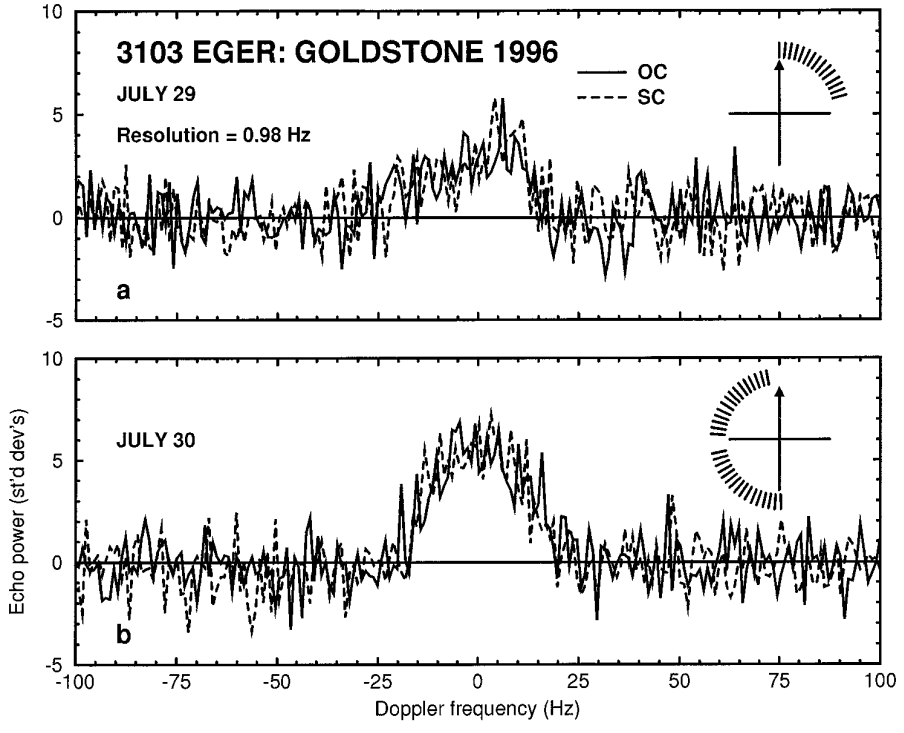

FIG. 11. Eger echo spectra from 1996. The zero-phase UTC epoch is at 1996 July 29 08:29:44. The relation between the zero-phase epochs in 1986, 1991, and 1996 is not known. Note the asymmetry of the July 29 spectra.

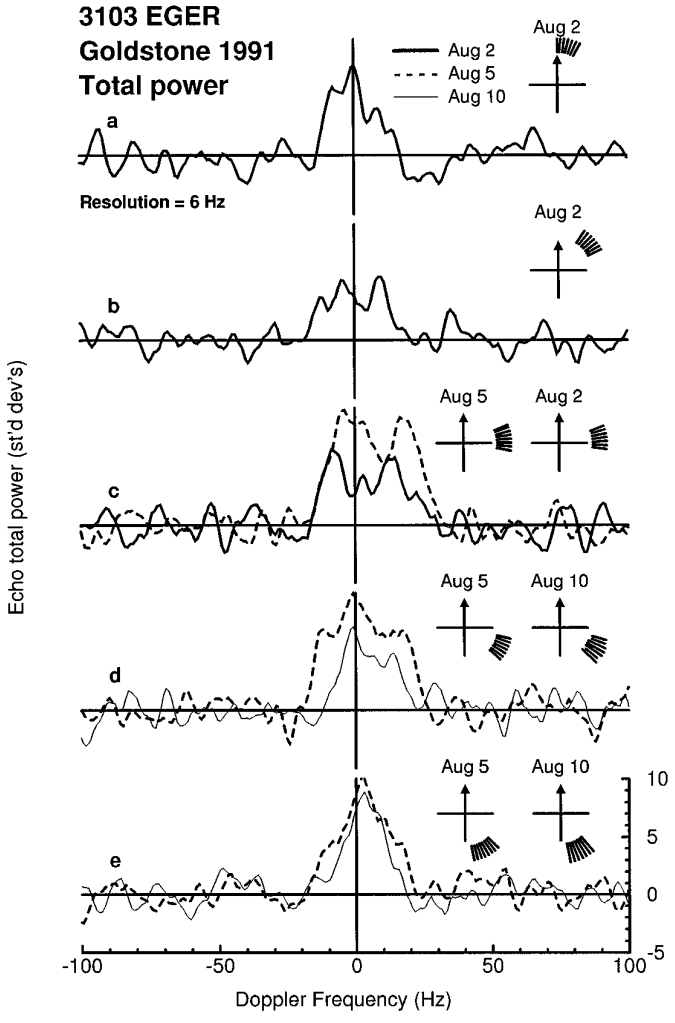

FIG. 12. Evolution of total power Eger spectra as a function of rotation phase in 1991. Each spectrum spans about 30° of rotation and is filtered to 6-Hz resolution.

4. POLARIZATION SIGNATURES OF ADONIS, EGER, AND 1992 QN

The near-unity circular polarization ratios of these objects (Table III) are the highest measured for any asteroid. The only other NEAs with measured circular polarization ratios in excess of 0.5 are 1981 Midas ($\mu_C = 0.65 \pm 0.13$, $\lambda = 3.5$ cm) and 3908 (1980 PA) ($\mu_C = 0.78 \pm 0.02$, $\lambda = 13$ cm; $\mu_C = 0.72 \pm 0.04$, $\lambda = 3.5$ cm) (Ostro *et al.* 1991a).

Anomalously large circular polarization ratios have also been observed in radar echoes from the icy Galilean satellites Europa, Ganymede, and Callisto (Ostro *et al.* 1992), the polar regions on Mars (Muhleman *et al.* 1991) and Mercury (Slade *et al.* 1992), and the Greenland ice cap (Rignot *et al.* 1993, Rignot 1995). Those particular polarization signatures may be due to volume scattering in clean water ice, with the coherent backscattering effect causing at least some enhancement of μ_C (Mishchenko 1996 and references therein). Near-unity polarization ratios have also been observed in radar echoes from a terrestrial basaltic andesite lava flow (Campbell *et al.* 1993), from Alpha Regio on Venus (Tryka and Muhleman 1992), at oblique angles from the volcanic Tharsis region on Mars (Harmon and Ostro 1985), and from steep radar-facing crater slopes on the moon (Stacy *et al.* 1997), and thus do not necessarily indicate an icy composition. SC echoes can be caused by multiple scattering or by single scattering from surfaces with radii of curvature comparable to the wavelength, so coherent backscattering is not their only source (Mishchenko 1996). Thus, although the circular polarization ratios and radar albedos of Adonis and 1992 QN may be comparable to those of Callisto ($\mu_C = 1.1$–1.3, $\hat{\sigma}_{OC} \approx 0.3$), the high circular polarization ratios observed from other non-icy terrains argue that $\mu_C \sim 1.0$ does not satisfy a necessary or sufficient condition for water ice.

For backscattering from natural targets, μ_C is expected to be at least as large as and usually a few times greater than μ_L (as is observed for Eger; Table III). In the context of the available rough-surface and coherent-backscatter literature, Adonis' combination of μ_C near unity and μ_L near zero seems very strange. On the other hand, realistic treatments of scattering from even simplified physical systems contain large spaces of parameters that might be adjustable to match the Adonis results. For example, Mishchenko (1996, p. 700) states that coherent backscattering can "increase the circular polarization ratio and either increase or decrease the linear polarization ratio." Thus, the degree to which coherent backscattering, or for that matter volume vs surface scattering, might be responsible for the polarization signatures of Adonis, Eger, and 1992 QN is an open question. What is clear is that the high circular-polarization ratios of these objects require extreme near-surface roughness at spatial scales within about an order of magnitude of the radar wavelength. As an example, high μ_C might result from multiple internal scattering from a blocky surface overlain by a low-loss, low-density regolith several decimeters thick. The source of the roughness is uncertain, although it probably involves the physics of impact cratering and debris retention on low-gravity objects.

Is Adonis an inactive comet nucleus? Drummond (1982) pointed out that the orbit of Adonis (Table I) is similar to those of several meteor streams and suggested that Adonis may be a dormant or extinct comet (see also Weissman *et al.* 1989). Asher *et al.* (1993) related Adonis to the Taurid complex, which consists of Comet Encke, several meteor streams, and several NEAs with similar orbits. Recently Valsecchi *et al.* (1995) identified a dynamical route that connects Jupiter family comets and some main-belt asteroids to the Taurid complex and apparently explains the presence of Comet Encke and several NEAs within the

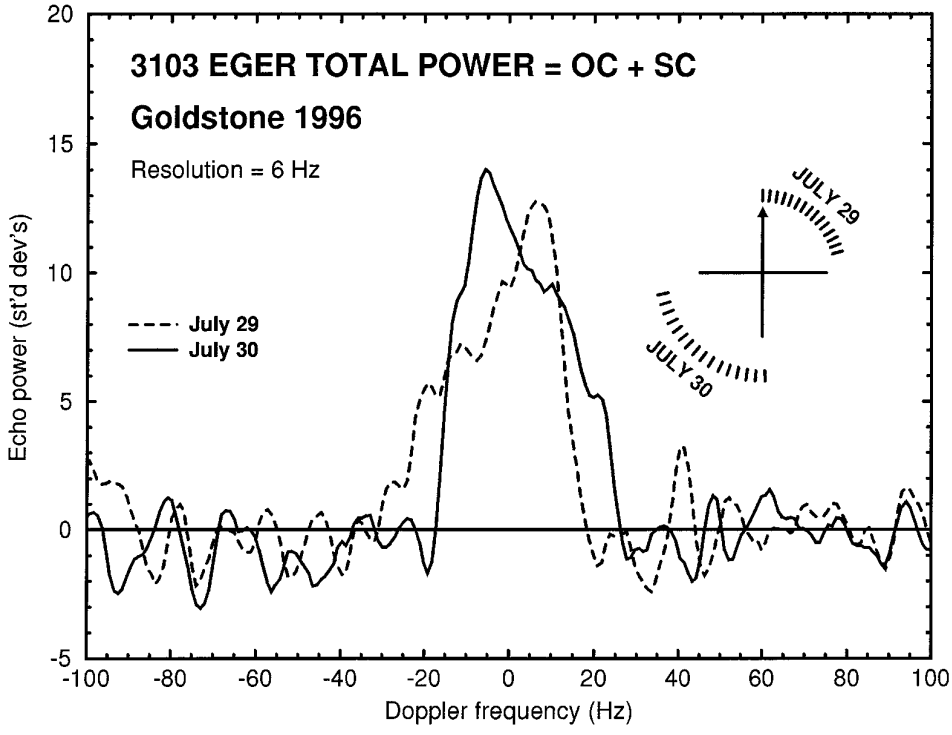

FIG. 13. Total power spectra obtained on opposite sides of Eger in 1996.

putative Taurid population. Adonis' Tisserand parameter (given by $T = a_J/a + 2 \cos i[(a/a_J)(1 - e^2)]^{1/2}$, where a_J is the semimajor axis of Jupiter, and a, e, and i are the semimajor axis, eccentricity, and inclination of the asteroid), which is <3 for ~90% of numbered Jupiter family comets and >3 for nearly 100% of numbered asteroids with $a <$ 3.3 AU, has a value $T = 3.55$, exceeding the largest known cometary value of $T = 3.18$ for P/1996 N2 Elst–Pizarro [orbital elements used to compute T were taken from the JPL Solar System Dynamics homepage at: http://ssd.jpl.nasa.gov/(Chamberlin *et al.* 1997)]. The orbital evolution of Adonis seems consistent with an origin either as a main-belt asteroid or as a Jupiter family comet, but its present orbit is not obviously cometary. No optical spectra are available, nor is there any evidence of cometary activity. Ostro (1985) and Weissman *et al.* (1989) suggested that Adonis' high circular polarization ratio might be due to the presence of water ice, but subsequent observations indicate that water ice is not required to produce high circular polarization ratios. Furthermore, we do not know what the radar properties of inactive cometary nuclei are, and comparisons with active cometary nuclei may not be meaningful because their radar properties may be very different. However, the radar properties of Adonis differ markedly from those of the active comets best studied by radar: C/1983 H1 IRAS–Araki–Alcock (Goldstein *et al.* 1984, Harmon *et al.* 1989), 26P/Grigg–Skjellerup (Kamoun 1983), and C/1996 B2 Hyakutake (Harmon *et al.* 1997) have lower mean circular polarization ratios ($\mu_C < 0.5$) and low radar albedos ($\hat{\sigma}_{OC} \leq 0.1$). Thus the existing radar observations do not provide compelling evidence either for or against a cometary origin of Adonis.

5. FUTURE RADAR OPPORTUNITIES

Table V lists observing opportunities for each asteroid at Arecibo and Goldstone during 1997–2020. Arecibo observations should yield echoes stronger than existing data by factors that range from two for Adonis to an order of magnitude for Aten and 1992 QN. Any of the opportunities with SNRs >20 should permit resolution of echoes in time delay. For Aten, Eger, and 1992 QN, the best opportunities should yield images adequate to construct crude shape models. Future observations certainly should improve upon our estimated polarization ratios.

ACKNOWLEDGMENTS

We thank the staff at the Arecibo Observatory and the Goldstone Radio Astronomy/Radar Group for technical assistance with the observations. Part of this research was conducted at the Jet Propulsion Laboratory, California Institute of Technology, under contract with NASA. Work at the Center for Astrophysics was supported in part by NASA. L. A. M. Benner was supported as a Research Associate of the National Research Council. The Arecibo Observatory is part of the National Astronomy and Ionosphere Center, which is operated by Cornell University under a cooperative agreement with the National Science Foundation and with support from NASA.

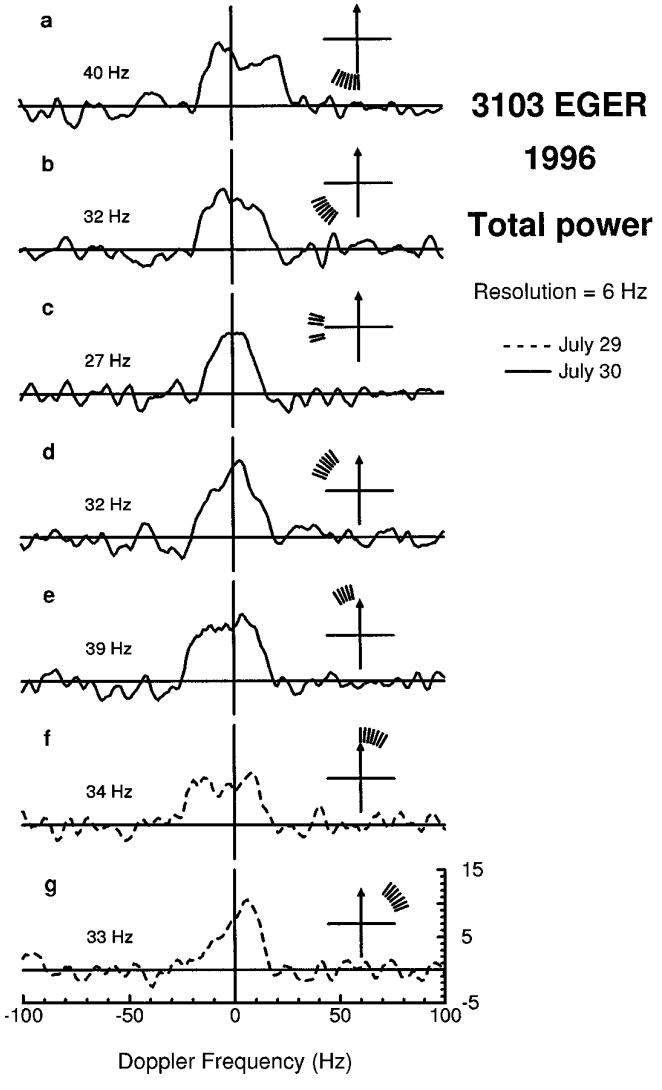

FIG. 14. Radar "movie" depicting the evolution of Eger total power spectra in 1996. Each spectrum was formed from a weighted sum of individual spectra covering 30° of rotation phase. Estimated bandwidths are indicated at the lower left in each panel.

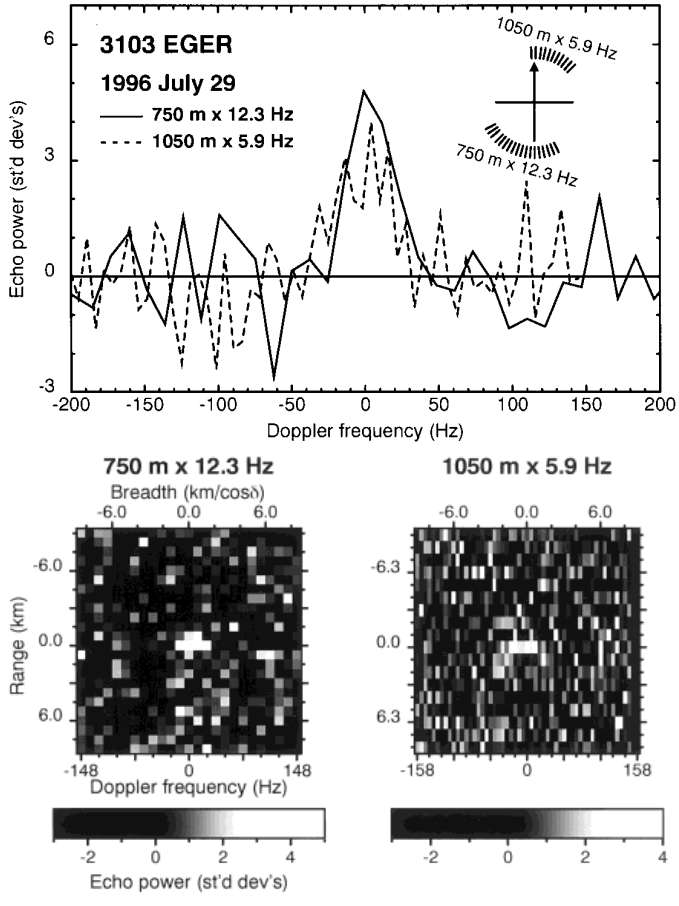

FIG. 15. Eger echo power spectra (top) extracted from 5 μs (750 m) $\times$ 12.3 Hz (bottom left) and 7 μs (1050 m) $\times$ 5.86 Hz (bottom right) delay-Doppler images obtained on 1996 July 29. Each image shows the distribution of echo power in standard deviations relative to Eger's estimated center-of-mass frequency and distance. The radar illuminates Eger from the top and range increases toward the bottom. Weighted sums in each image of ~6 contiguous pixels with echo power exceeding the 2-sigma level achieve SNRs of ~7, yielding a delay estimate of 133,166,634 $\pm$ 10 μs at the epoch: 1996 July 29 13:00:00 UTC. The 1996 radar astrometry shrinks the 1-sigma plane-of-sky error ellipse area at the time of Eger's next close encounter in 2001 by ~40% and reduces standard errors in Eger's radial position and velocity vector components by about a factor of two. Echo power spectral points from the radar image with resolution cells of 750 m $\times$ 12.3 Hz are weighted sums taken from the two range rows that contain echoes. The 1050 m $\times$ 5.86 Hz resolution echo power spectrum is taken from the one row containing echoes.

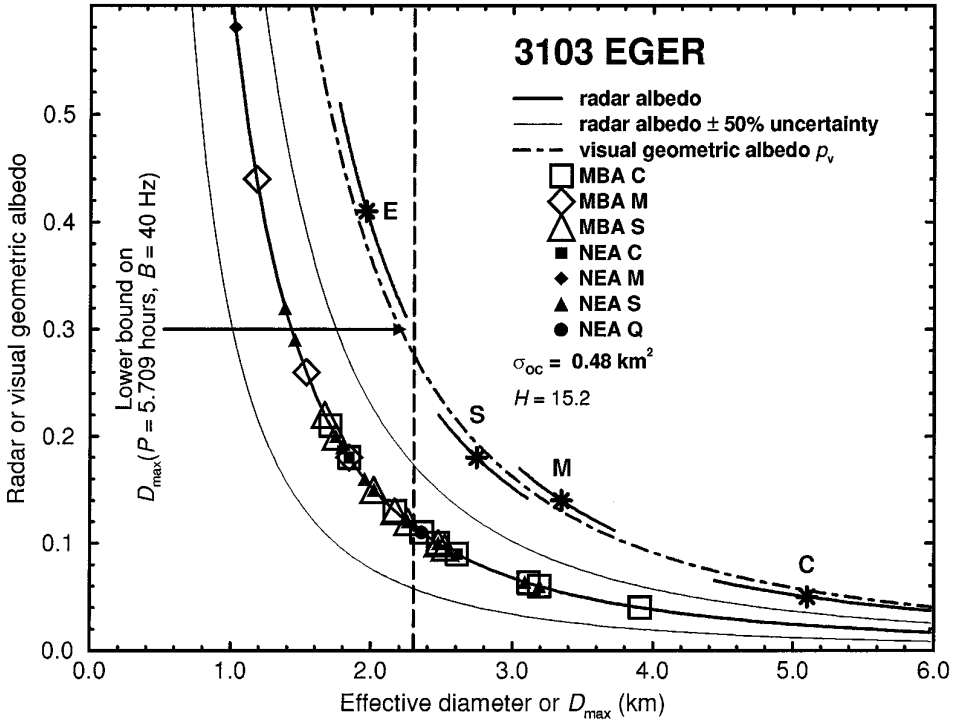

FIG. 16. Constraints on Eger's diameter and radar and geometric albedos. Eger's maximum bandwidth (Table III) and rotation period (Table I) establish a lower bound on its maximum pole-on breadth D_{max} = 2.3 km.

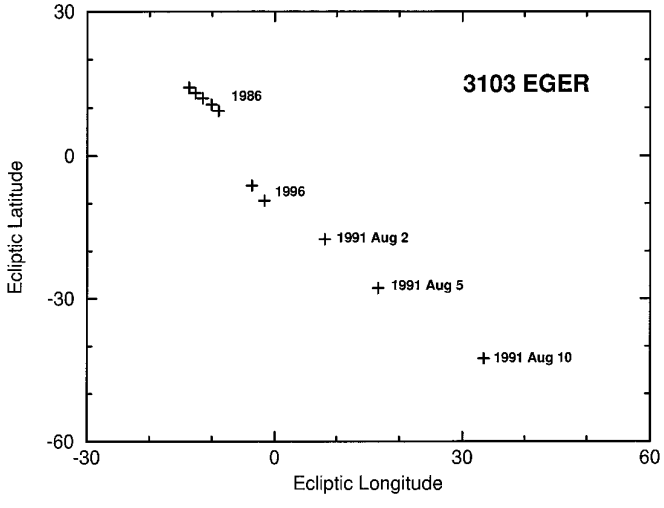

FIG. 17. Ecliptic positions of Eger in 1986, 1991, and 1996.

TABLE V
Future Radar Opportunities: 1997–2020

TARGET		DATE	Distance (AU)	Arecibo SNR	Goldstone SNR
2062	Aten	2012	0.24	30	
		2013	0.25	30	
		2014	0.15	220	10
		2015	0.19	70	
2101	Adonis	2002	0.17	30	
		2018	0.22	10	
3103	Eger	2001	0.16	200	50
		2006	0.17	190	30
		2011	0.19	130	20
		2016	0.22	80	10
4544	Xanthus	2006	0.23	30	
		2007	0.20	50	
	1992 QN	2005	0.26	40	
		2009	0.21	110	
		2018	0.25	50	

Note. Predictions for future observations in which the OC SNR per day exceeds 10 for nominal parameters of the upgraded Arecibo telescope.

REFERENCES

Asher, D. J., S. V. M. Clube, and D. I. Steel 1993. Asteroids in the Taurid complex. *Mon. Not. R. Astron. Soc.* **264,** 93–105.

Campbell, B. A., R. E. Arvidson, and M. K. Shepard 1993. Radar polarization properties of volcanic and playa surfaces: Applications to terrestrial remote sensing and Venus data interpretation. *J. Geophys. Res.* **98,** 17,099–17,113.

Chamberlin, A. B., D. K. Yeomans, P. W. Chodas, J. D. Giorgini, R. A. Jacobson, M. S. Keesey, J. H. Lieske, S. J. Ostro, E. M. Standish, and R. N. Wimberly 1997. JPL Solar System dynamics WWW site. *Bull. Am. Astron. Soc.* **29,** 1014. [Abstract]

Chapman, C. R., A. W. Harris, and R. Binzel 1994. Physical properties of near-Earth asteroids: Implications for the hazard issue. In *Hazards Due to Comets and Asteroids* (T. Gehrels, Ed.), pp. 537–549. Univ. of Arizona Press, Tucson.

Cruikshank, D. P., and T. J. Jones 1977. The diameter and albedo of asteroid 1976 AA. *Icarus* **31,** 427–429.

Drummond, J. D. 1982. Theoretical meteor radiants of Apollo, Amor, and Aten asteroids. *Icarus* **49,** 143–153.

Gaffey, M. J., K. L. Reed, and M. S. Kelley 1992. Relationship of E-type Apollo asteroid 3103 (1982 BB) to the enstatite achondrite meteorites and the Hungaria asteroids. *Icarus* **100,** 95–109.

Goldstein, R. M., R. F. Jurgens, and Z. Sekanina 1984. A radar study of Comet IRAS–Araki–Alcock 1983d. *Astron. J.* **89,** 1745–1754.

Gradie, J. C. 1976. Physical observations of object 1976 AA. *Bull. Am. Astron. Soc.* **8,** 458. [Abstract]

Harmon, J. K., and S. J. Ostro 1985. Mars: Dual-polarization radar observations with extended coverage. *Icarus* **62,** 110–128.

Harmon, J. K., D. B. Campbell, A. A. Hine, I. I. Shapiro, and B. G. Marsden 1989. Radar observations of Comet IRAS–Araki–Alcock 1983d. *Astrophys. J.* **338,** 1071–1093.

Harmon, J. K., S. J. Ostro, L. A. M. Benner, K. D. Rosema, R. F. Jurgens, R. Winkler, D. K. Yeomans, D. Choate, R. Cormier, J. D. Giorgini, D. L. Mitchell, P. W. Chodas, R. Rose, D. Kelley, M. A. Slade, and M. L. Thomas 1997. Radar detection of the nucleus and coma of Comet Hyakutake (C/1996 B2). *Science*, in press.

Helin, E. F., and E. M. Shoemaker 1977. Discovery of asteroid 1976 AA. *Icarus* **31,** 415–419.

Kamoun, P. G. D. 1983. *Radar Observations of Cometary Nuclei*. Ph.D. thesis, Massachusetts Institute of Technology.

Marsden, B. G. 1996. *Minor Planet Circ.* No. 27729.

Meisel, D. D., V. S. Getman, J. D. Mathews, S. C. Jacobs, and R. G. Roper 1995. Bolide AIDA: Death of an aubrite meteoroid. *Icarus* **116,** 227–254.

Milani, A., M. Carpino, G. Hahn, and A. M. Nobili 1989. Dynamics of planet-crossing asteroids: Classes or orbital behavior. Project SPACEGUARD. *Icarus* **78,** 212–269.

Mishchenko, M. I. 1996. Diffuse and coherent backscattering by discrete random media. I. Radar reflectivity, polarization ratios, and enhancement factors for a half-space of polydisperse, nonabsorbing and absorbing spherical particles. *J. Quant. Spectrosc. Radiat. Trans.* **56,** 673–702.

Mitchell, D. L., S. J. Ostro, K. D. Rosema, R. S. Hudson, D. B. Campbell, J. F. Chandler, and I. I. Shapiro 1995. Radar observations of asteroids 7 Iris, 9 Metis, 12 Victoria, 216 Kleopatra, and 654 Zelinda. *Icarus* **118,** 105–131.

Mitchell, D. L., S. J. Ostro, R. S. Hudson, K. D. Rosema, D. B. Campbell, R. Vélez, J. F. Chandler, I. I. Shapiro, J. D. Giorgini, and D. K. Yeomans 1996. Radar observations of asteroids 1 Ceres, 2 Pallas, and 4 Vesta. *Icarus* **124,** 113–133.

Morrison, D., J. C. Gradie, and G. H. Reike 1976. Radiometric diameter and albedo of the remarkable asteroid 1976 AA. *Nature* **260,** 691.

Mottola, S., G. de Angelis, M. Di Martino, A. Erikson, G. Hahn, and G. Neukum 1995. The near-Earth objects follow-up program: First results. *Icarus* **117,** 62–70.

Muhleman, D. O., B. J. Butler, A. W. Grossman, and M. A. Slade 1991. Radar images of Mars. *Science* **253,** 1508–1513.

Ostro, S. J. 1985. Radar observations of asteroids and comets. *Publ. Astron. Soc. Pacific* **97,** 877–884.

Ostro, S. J. 1993. Planetary radar astronomy. *Rev. Mod. Phys.* **65,** 1235–1279.

Ostro, S. J., D. B. Campbell, and I. I. Shapiro 1985. Mainbelt asteroids: Dual-polarization radar observations. *Science* **229,** 442–446.

Ostro, S. J., D. K. Yeomans, P. W. Chodas, R. M. Goldstein, R. F. Jurgens, and T. W. Thompson 1989. Radar observations of asteroid 1986 JK. *Icarus* **78,** 382–394.

Ostro, S. J., D. B. Campbell, J. F. Chandler, I. I. Shapiro, A. A. Hine, R. Velez, R. F. Jurgens, K. D. Rosema, R. Winkler, and D. K. Yeomans 1991a. Asteroid radar astrometry. *Astron. J.* **102,** 1490–1502.

Ostro, S. J., D. B. Campbell, J. F. Chandler, A. A. Hine, R. S. Hudson, K. D. Rosema, and I. I. Shapiro 1991b. Asteroid 1986 DA: Radar evidence for a metallic composition. *Science* **252,** 1399–1404.

Ostro, S. J., D. B. Campbell, R. A. Simpson, R. S. Hudson, J. F. Chandler, K. D. Rosema, I. I. Shapiro, E. M. Standish, R. Winkler, D. K. Yeomans, R. Velez, and R. M. Goldstein 1992. Europa, Ganymede, and Callisto: New radar results from Arecibo and Goldstone. *J. Geophys. Res.* **97,** 18,277–18,244.

Ostro, S. J., L. A. M. Benner, D. Choate, C. R. Franck, R. Frye, J. D. Giorgini, D. Howard, R. F. Jurgens, D. Kelley, D. L. Mitchell, R. Rose, K. D. Rosema, M. A. Slade, R. Winkler, D. K. Yeomans, and R. S. Hudson 1996a. Near-Earth-object radar astronomy at Goldstone in 1996. *Bull. Am. Astron. Soc.* **28,** 1105. [Abstract]

Ostro, S. J., R. F. Jurgens, K. D. Rosema, R. S. Hudson, J. D. Giorgini, R. Winkler, D. K. Yeomans, D. Choate, R. Rose, M. A. Slade, S. D. Howard, D. J. Scheeres, and D. L. Mitchell 1996b. Radar observations of asteroid 1620 Geographos. *Icarus* **121,** 46–66.

Rignot, E. 1995. Backscatter model for the unusual radar properties of the Greenland ice sheet. *J. Geophys. Res.* **100,** 9389–9400.

Rignot, E. J., S. J. Ostro, J. J. van Zyl, and K. C. Jezek 1993. Unusual radar echoes from the Greenland ice sheet. *Science* **261,** 1710–1713.

Shoemaker, C. S., E. M. Shoemaker, H. E. Holt, and N. G. Thomas 1989. *IAU Circ.* 4766.

Slade, M. A., B. J. Butler, and D. O. Muhleman 1992. Mercury radar imaging: Evidence for polar ice. *Science* **258,** 635–640.

Stacy, N. J. S., D. B. Campbell, and P. G. Ford 1997. Arecibo radar mapping of the lunar poles: A search for ice deposits. *Science* **276,** 1527–1530.

Tedesco, E. F. 1989. Asteroid magnitudes, UBV colors, and IRAS albedos and diameters. In *Asteroids II* (R. P. Binzel, T. Gehrels, and M. S. Matthews, Eds.), pp. 1090–1138. Univ. of Arizona Press, Tucson.

Tedesco, E. 1990. *Minor Planet Circ.* No. 17264.

Tedesco, E. 1990. *Minor Planet Circ.* No. 17272.

Tholen, D. J., and M. A. Barucci 1989. Asteroid taxonomy. In *Asteroids II* (R. P. Binzel, T. Gehrels, and M. S. Matthews, Eds.), pp. 298–315. Univ. of Arizona Press, Tucson.

Tryka, K. A., and D. O. Muhleman 1992. Reflection and emission properties on Venus: Alpha Regio. *J. Geophys. Res.* **97,** 13,379–13,394.

Valsecchi, G. B., A. Morbidelli, R. Gonczi, P. Farinella, Ch. Froeschlé, and Cl. Froeschlé 1995. The dynamics of objects in orbits resembling that of P/Encke. *Icarus* **118,** 169–180.

Veeder, G. J., M. S. Hanner, D. L. Matson, E. F. Tedesco, L. A. Lebofsky, and A. T. Tokunaga 1989. Radiometry of near-Earth asteroids. *Astron. J.* **97,** 1211–1219.

Weissman, P. R., M. F. A'Hearn, L. A. McFadden, and H. Rickman 1989. Evolution of comets into asteroids. In *Asteroids II* (R. P. Binzel, T. Gehrels, and M. S. Matthews, Eds.), pp. 880–920. Univ. of Arizona Press, Tucson.

Wisniewski, W. Z. 1987. Photometry of six radar target asteroids. *Icarus* **70,** 566–572.

Wisniewski, W. Z. 1991. Physical studies of small asteroids. I. Lightcurves and taxonomy of 10 asteroids. *Icarus* **90,** 117–122.

Zellner, B. 1979. Asteroid taxonomy and the distribution of the compositional types. In *Asteroids* (T. Gehrels, Ed.), pp. 783–806. Univ. of Arizona Press, Tucson.